# Stony Brook University

# Residual Stress Measurements of NiCr, Molybdenum, Tungsten, and Silver Thermally Sprayed Coatings using X-Ray Methodology

A Thesis Presented

By

**Joseph C. Japson**

To

The Graduate School

In Partial fulfillment of the

Requirements

For the Degree of

**Master of Science**

**in**

**Materials Science and Engineering**

Stony Brook University

May 2008

**Stony Brook University**

The Graduate School

**Joseph C. Japson**

We, the thesis committee for the above candidate for the

Master of Science degree,

hereby recommend acceptance of this thesis.

Dr. Sanjay Sampath, Advisor
Department of Materials Science and Engineering

Dr. Andrew Gouldstone
Department of Materials Science and Engineering

Dr. Richard Gambino
Department of Materials Science and Engineering

This thesis is accepted by the Graduate School

Lawrence Martin
Dean of the Graduate School

Abstract of the Thesis

**Residual Stress Measurement of NiCr, Molybdenum, Tungsten, and Silver Thermally Sprayed Coatings using X-Ray Methodology**

By

Joseph C. Japson

Master of Science

in

Materials Science and Engineering

Stony Brook University

2008

A brief overview of how x-ray diffraction is used to obtain residual stress measurements in thermally sprayed coatings will be discussed. Four NiCr process map coatings sprayed with HVOF process will be discussed and compared, as well as two coatings done with Air Plasma Spray (APS), Ag and W. The residual stress measurements between the HVOF and APS coatings will be compared to one another. Comparisons of residual stress from curvature and x-ray methods are also evaluated from the four parameters of NiCr coating. This report used the

$\sin^2\Psi$ x-ray diffraction method to obtain the residual stress for both APS and HVOF coatings.

A second study between the relationship of substrate surface roughness and its influence on residual stress from thermally sprayed systems will also be evaluated. Four different substrate parameters were investigate these being; polished (600grit-paper), as received, 40psi Alumina grit-blast, and 80psi Alumina grit-blast. Two coatings were used in this second investigation, one being NiCr and the other Mo. The NiCr coating was deposited using the HVOF process while the Mo coatings were made via APS. There were two sets of Mo experiments conducted because to see whether substrate residual stress, prior to spraying, played any role in the final coating/substrate residual stress.

This thesis has examined the differences between HVOF and APS residual stress due to the different characteristics of each process. HVOF coatings have dissimilar coating structures than that of APS resulting in unrelated residual stress states. It seems that the APS process creates columnular grain orientation thus greatly affecting its residual stress outcome especially when using XRD methodology. On the other hand, the HVOF process does not create these preferred grain orientations and has therefore shown produces acceptable XRD results. Further investigation on how these particular grains are created is vital to understanding the final coating properties and stress in the APS process.

*This thesis is dedicated to my parents and sisters*

# Table of Contents

# List of Figures

# List of Tables

# Acknowledgment

First and foremost I would like to acknowledge Dr. Sanjay Sampath kind generosity and words of wisdom provided throughout my years at Stony Brook. Many thanks to the Center for Thermal Spray Research group for providing me the opportunity to perform my scientific research. Special thanks go to the thermal spray operators who helped me create my research samples without them I would not be able to conduct my thesis report. Thanks to Dr. Andrew Gouldstone and Eileen Zappia for their guidance and knowledge throughout the years.

I would also like to thank the personnel at the Institute of Plasma Physics, Prague, Czech Republic, especially Mr. Jiri Matejick and Mr. Jiri Dubsky for providing their expertise, specifically x-ray diffraction and the operational use of the x-ray diffractometer at IPP. These two fine gentlemen not only helped me in my research, but also provided direction and hospitality during my stay in the Czech Republic.

Finally, I'd like to express deep gratitude to my parents and family, without there love and support I would not be where I am today. Thank you all.

# Chapter 1: Introduction

Stress that remains in the material after the original cause of the stress has been removed is known as residual stress. Residual stress occurs for a variety of reasons, including inelastic deformations and heat treatment, especially in the case of thermal spray. The cooling of thermally sprayed material onto substrates causes some layers to contract more than others, leaving residual stresses. While uncontrolled residual stresses are undesirable, many designs rely on them; for examples toughened glass and pre-stressed concrete. Therefore, it is important to understand and control the amount of residual stress applied to a material.

The origin of a particular residual stress state depends on the type of thermal spray process the part has undergone. The thermal spray process causes a rapid quenching of the molten droplets upon impact on the substrate with restricted contraction [1]. This temperature drop is approximately 2000°C and would lead to tensile stress from the splat quenching to the substrate immediately during impact. The cooling of the entire deposited coating and substrate from deposition to room temperature is another origin of residual stress in coatings. The difference in each materials coefficient of thermal expansion gives rise to residual stress and is called the thermal mismatch stress. This thermal mismatch stress can either be compressive or tensile, depending on the difference in magnitude of the thermal contraction between the two components. The peening

effect, or compressive stress cause by unmelted particles impacting the substrate, can also provide residual stresses in the coating and has been found in the HVOF process [6].

Since particle velocity for the HVOF process is much higher than other spray processes, compressive residual stress is more prevalent in this spray procedure. Each newly deposited layer adds compressive stresses to the previously deposited layer. The relieving mechanisms of residual stress for the substrate/coating system are: yielding, microcracking, creep, edge relaxation, and interfacial sliding. Consequently, it is important to recognize the thermal spray process of a coating so that a better understanding of what type of residual stresses can be found within it and modify the spray process to create a more positive condition.

Residual stress measurements in coatings are commonly done via the material removal method, substrate curvature measurement, and diffraction method (either by X-ray or neutron) [4]. Each method has there own positive and negative advantages, but this investigation primarily deals with the X-ray diffraction method.

Material removal is capable of obtaining through-thickness stress gradients, through the use of strain gauges, since it either drills a hole in the coating/substrate or grinds off a coating layer. The drawback to this method is that is can damage the coating, induce stress, and is difficult to control the

uniformity of material removal. Substrate curvature uses either optical or mechanical measurement of the component to directly measure substrate/coating stress. It is capable of observing stress changes in during deposition and is capable of identifying the quenching and thermal mismatch stresses. The disadvantage of this measurement method is that it can determine only average stress value in the substrate/coating system, and has limitations on specimen shape and dimensions [1].

X-ray diffraction (XRD) is a useful tool for measuring the change in d-spacing of a crystalline material. This information can then be used to obtain the stresses that are within it. X-ray diffraction is limited in the depth that it is capable of penetrating a material, in the order of tens of microns deep. As a result, it is suitable for thick film coatings, such as the ones produced by the thermal spray process. XRD is a nondestructive way to measure residual stress, it is phase distinctive, is able to measure various types of shapes and sizes of samples.

Stress determination by means of neutron diffraction is based on the same principle as X-ray diffraction, except neutrons can penetrate into a depth of the order of mm or cm in common materials; therefore, data can be collected from inside the material, as opposed to X-rays which are limited to thin surface layer. High penetration of neutrons is probably the most important advantage – it enables non-destructive determination of triaxial stress profiles inside specimens

of complex shapes, in coatings as well as substrates, and is not affected by surface finish. Among the drawbacks are lower spatial resolution, demanding experimental procedure and limited availability of the instruments [5].

## 1.1 Thick Film Coatings via Thermal Spray Process

The thermal spray process produces molten droplets of a particular material or alloy to be deposited on to a substrate with such high velocity (70m/s for APS and even more for HVOF process) at temperatures commonly 3000F or C such that you create splat or pancakes. These splats are deposited over several layers to create a coating with thickness ranging from microns to millimeters. This causes a lot of stress during the impact with the substrate material and so understanding the stresses of the final coating/substrate system is critical. It is possible to have either a tensile or compressive residual stress state in your final film coating depending on certain factors that I will be discussing in this paper. The molten particles spread like a pancakes over the substrate, then cool rapidly and finally solidify. This creates a great amount of stress on the substrate and so understanding and being able to manipulate such residual stress can be extremely valuable in the materials processing industry.

## 1.2 Residual Stress Measurement via XRD Methodology

As mentioned above, XRD measures the crystal plane spacing in a given direction, determined from the peak position using Bragg's law [7]:

$$n\,\lambda = 2\,d\,\sin\theta \tag{1}$$

where $n$ is the reflection order, $\lambda$ is the radiation wavelength, $d$ is the plane spacing and $\theta$ is the diffraction angle. The strain is then given by [7]

$$\varepsilon = (d - d_0) / d_0 = -\cot\theta(\theta - \theta_o) \tag{2}$$

where $\varepsilon$ is the strain in a particular direction, $d$ is the stressed and $d_0$ the unstressed interplanar spacing. Similarly, $\theta$ is the stressed diffraction angle and $\theta_o$ is the unstressed diffraction angle. The general relationship between strain and stress is as follows [5]:

$$\varepsilon_{ij} = 1/2\,S_2\,\sigma_{ij} + \delta_{ij}\,S_1(\sigma_{XX} + \sigma_{YY} + \sigma_{ZZ}) \tag{3}$$

$\varepsilon_{ij}$ being components of the elastic strain tensor, $\sigma_{ij}$ components of the stress tensor in the specimen coordinate system, $\delta_{ij} = 1$ for i = j, $\delta_{ij} = 0$ for i ≠ j, $1/2S_2$ and $S_1$ are so called crystallographic elastic constants. For isotropic materials, they are related to Young's modulus ($E$) and Poisson's ratio ($\nu$) through the following relationship:

$$1/2\,S_2 = (1 + \nu) / E \quad \text{and} \quad S_1 = -\nu / E \tag{4}$$

Common practice recommends at least eight measurements in different orientations are necessary for the determination of all independent stress tensor

components. Specimen geometry and physical state give rise to application of some assumptions that can minimize the number of orientation measurements [3]. This experiment used ten measurements in different orientations for all six specimens.

The "$\sin^2\psi$" method is commonly used in XRD measurement because of the low penetration of x-rays. The low penetration makes use of the zero normal stress condition and does not require a stress-free reference $d_0$. This method uses sample tilting around the axis perpendicular to the path of the beam enabling d-spacing measurement in different orientations. The "$\sin^2\psi$" method uses a simplified version of equation (3):

$$\varepsilon = 1/2\, S_2\, \sigma_\varphi \sin^2\psi + S_1\, (\sigma_{XX} + \sigma_{YY}) \tag{5}$$

with

$$\sigma_\varphi = \sigma_{XX} \cos^2\varphi + \sigma_{XY} \sin 2\varphi + \sigma_{YY} \sin^2\varphi \tag{6}$$

where the angles $\psi$ and $\varphi$ denote the measurement direction; $\psi$ is the angle between sample surface normal and crystal plane normal, $\varphi$ the azimuthal angle in the surface plane. The subscripts *x, y, z* represent the sample coordinate system, where *x* and *y* are in the coating and *z* is perpendicular to the coating surface [3]. This particular XRD method was used to obtain residual stress measurements for my research.

# Chapter 2: Experimental Procedures

## 2.1 Thermal Spray Details

Coatings of all specimens were prepared and sprayed at the Center for Thermal Spray Research at Stony Brook, NY, USA. A water cooled HVOF DJ-Gun 2700 from Sulzer-Metco with propylene as fuel was used to fabricate the NiCr coatings. Figure 1 shows the set up for the HVOF experiment.


*Fig. 1. Water cooled HVOF DJ-Gun 2700 at the Center for Thermal Spray Research at Stony Brook University, NY*

Four different spray conditions were deposited over beam samples. Low carbon steel beams of 228.6 mm (9 in.) length, 25.4 mm (1 in.) width and 1.59 mm (1/16 in.) thickness grit blasted on both sides were used as substrates. Ni-20%Cr powder from Praxair, San Ramon, CA, (particle size -45 μm/+5 μm) was used to spray coatings at a constant rate of 23 g/min. Fifteen passes were sprayed in the four experiments.

One set of two beams (A and B) was sprayed varying the fuel/oxygen volume flow ratio at 0.22 stoichiometric and 0.38 reducing (fuel-rich) conditions while keeping constant the total volume flow at ~1315 SCFH. A second set of two beams (C and D) was sprayed at a lower total volume flow at ~1284 SCFH at 0.22 and 0.30 fuel to oxygen ratios [6]. Tables 1 and 2 show the values of each different parameter used in this NiCr experiment.

| Id. | Fuel/ Oxygen | Total Vol. Flow | Temp. | Veloc. |
|---|---|---|---|---|
| | | SCFH | ºC | m/s |
| A | 0.22 | 1315 | 2134±20.1 | 736±5.1 |
| B | 0.38 | 1315 | 1806±16.4 | 797±5.8 |
| C | 0.22 | 1284 | 2204±26.9 | 766±4.2 |
| D | 0.30 | 1284 | 2095±36.0 | 822±7.1 |

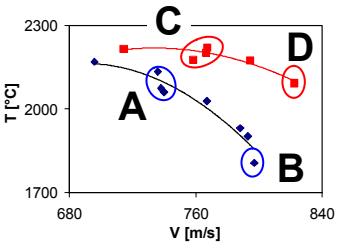


*Table 1. Ni20Cr Coatings: T-V average values and standard deviation* [6]

| Id. | Max. Surface Spray Temp. | Deposition Efficiency | Coating Thickness | Substrate Thickness |
|---|---|---|---|---|
| | ºC | % | mm | mm |
| A | 218.12 | 0.47 | 0.3066 | 1.618 |
| B | 319.16 | 0.52 | 0.3700 | 1.624 |
| C | 226.74 | 0.45 | 0.3100 | 1.620 |
| D | 273.77 | 0.45 | 0.3056 | 1.625 |

*Table 2. Ni20Cr Coatings: Maximum surface spray temperature, deposition efficiency, and average values of coating and substrate thicknesses* [6]

A water cooled APS Gun with propylene as fuel was used to fabricate the Tungsten, Silver and Mo coatings. The W and Ag coatings were used in first experiment, comparing HVOF and APS residual stress states while the Mo coating was used in the second experiment, comparing substrate surface roughness and residual stress.

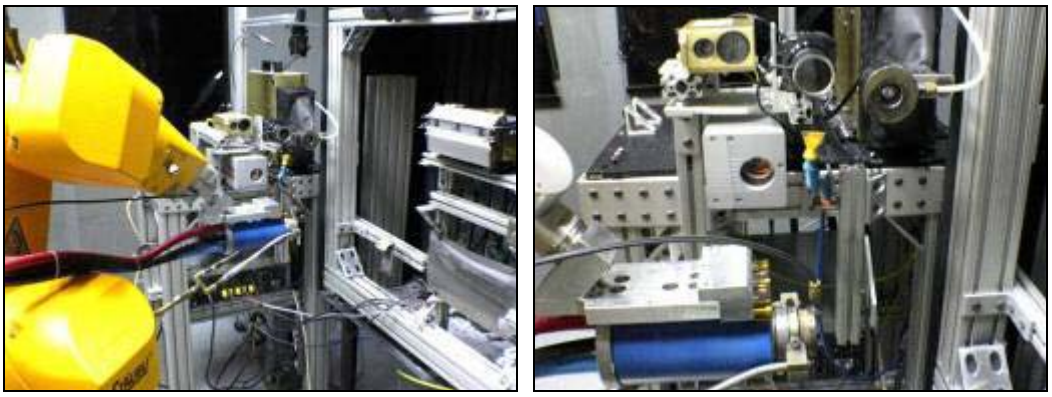

*Fig. 2. Air Plasma Spray Gun with sensor diagnostics and curvature box at the Center for Thermal Spray Research at Stony Brook University, NY*

Figure 2 shows the experimental setup for the APS gun at Stony Brook University. The figure on the left shows the robot arm, particle/plume sensors, and curvature box (from left to right). The image on the right shows the APS gun and the particle and plume sensors (bottom to top). The particle sensors are able to report particle velocity and temperature while the plume sensor detects plume size and intensity. The curvature box is used to measure the change in curvature of a substrate as it is being deposited with a thermal spray coating. The curvature box also helps determine modulus and stress of a coating.

## 2.2 X-ray Diffractometer Details

The X-ray analyses of samples were done in Prague, CZ, at the Institute of Plasma Physics using the Siemens D500 XRD machine. A Ni-filter was used on a CuKa1 X-ray tube source at 40kV and 25mA power supply. Typical run time for the different samples were anywhere from 14 to 18 hrs of operation. The NiCr

samples took about 18hrs while the Mo, Ag and W samples were only 14hrs of operation time. A curve fitting program, Turbobasic, was used to obtain the peak position of the various orientations of the sample and then stress calculations were done on Microsoft Excel.


*Fig. 3. X-ray Diffractometer D500 at the Institute of Plasma Physics, Prague, CZ*

The experimental parameters for the XRD machine for the six samples can be seen from the Table 3 containing tilt angle, steps per angle, and time per step. The table also includes the $2\theta$ position with deviations for each respective tilt angle both positive and negative. The sample tilt angles, $\Psi$, used in the experiments were selected as to cover enough of the sample with various tilt angles. It is usually evenly spaced because you want to give enough weight to each angle while also rotating enough of the sample to obtain good XRD measurements. The only criteria that $\Psi$ must satisfy is that it has to be lower than half of the lower range of the diffraction angle. From Table 3, it can be seen that

the tilt angles are the same for all NiCr coatings, but different from that of W and Ag because of the difference in lower range diffraction angle.

| Sample | Ψ(Tilt) | Steps | Time (sec) | (+) 2θ | (+)δθ | (-) 2θ | (-)δθ |
|---|---|---|---|---|---|---|---|
| **NiCr A (420) HVOF** | 0 | .02 | 40 | 152.314 | 0.0480 | 152.330 | 0.0371 |
| | 26 | .02 | 45 | 152.216 | 0.0510 | 152.260 | 0.0400 |
| | 38 | .02 | 55 | 152.134 | 0.0531 | 152.144 | 0.0530 |
| | 49 | .02 | 60 | 151.969 | 0.0586 | 152.120 | 0.0470 |
| | 60 | .02 | 70 | 151.862 | 0.0669 | 151.989 | 0.0580 |
| **NiCr B (420) HVOF** | 0 | .02 | 40 | 152.043 | 0.0430 | 152.008 | 0.0368 |
| | 26 | .02 | 45 | 151.836 | 0.0450 | 151.859 | 0.0320 |
| | 38 | .02 | 55 | 151.798 | 0.0430 | 151.776 | 0.0460 |
| | 49 | .02 | 60 | 151.586 | 0.0450 | 151.630 | 0.0430 |
| | 60 | .02 | 70 | 151.559 | 0.0510 | 151.679 | 0.0470 |
| **NiCr C (420) HVOF** | 0 | .02 | 40 | 152.626 | 0.0560 | 152.522 | 0.0620 |
| | 26 | .02 | 45 | 152.348 | 0.0630 | 152.367 | 0.0530 |
| | 38 | .02 | 55 | 152.352 | 0.0670 | 152.390 | 0.0550 |
| | 49 | .02 | 60 | 152.169 | 0.0620 | 152.218 | 0.0600 |
| | 60 | .02 | 70 | 152.044 | 0.0680 | 152.070 | 0.0640 |
| **NiCr D (420) HVOF** | 0 | .02 | 40 | 152.203 | 0.0430 | 152.192 | 0.0450 |
| | 26 | .02 | 45 | 152.057 | 0.0460 | 152.086 | 0.0440 |
| | 38 | .02 | 55 | 152.019 | 0.0450 | 152.027 | 0.0470 |
| | 49 | .02 | 60 | 151.794 | 0.0520 | 151.916 | 0.0480 |
| | 60 | .02 | 70 | 151.677 | 0.0580 | 151.868 | 0.0550 |
| **W (321) APS** | 0 | .04 | 20 | 131.210 | 0.0009 | 131.211 | 0.0009 |
| | 25 | .04 | 20 | 131.171 | 0.0011 | 131.225 | 0.0010 |
| | 35 | .04 | 25 | 131.169 | 0.0018 | 131.230 | 0.0020 |
| | 45 | .04 | 30 | 131.157 | 0.0026 | 131.238 | 0.0040 |
| | 55 | .04 | 35 | 131.136 | 0.0055 | 131.227 | 0.0068 |
| **Ag (333 and 511) APS** | 0 | .06 | 10 | 156.778 | 0.0030 | 156.770 | 0.0037 |
| | 20 | .06 | 20 | 156.753 | 0.0030 | 156.776 | 0.0029 |
| | 35 | .06 | 25 | 156.738 | 0.0025 | 156.772 | 0.0027 |
| | 50 | .06 | 30 | 156.712 | 0.0032 | 156.765 | 0.0024 |
| | 65 | .06 | 35 | 156.730 | 0.0042 | 156.811 | 0.0048 |

*Table 3. Coating specimen shown with different tilt angles, step per angle, time per step, 2θ positions, spray process and crystal plane orientation*

The determination of a suitable diffraction peak at high angle for the different material coating is also important when undergoing XRD measurements. Appropriate selection of the high angle diffraction peaks have several criteria to consider, since diffraction peaks are more sensitive at high angles. This means peak shifts will be more noticeable at higher angles than their lower angle counterparts; alternatively, the change in d-spacing will be more evident in a sample with similar strain throughout. A narrow peak at high angles is also important because it is easier to determine a peak shift when the width of the peak is not so wide. Unfortunately, high angles give weight to broader peaks so it is important to choice a peak that is not too broad with a large enough diffraction angle. Also, since XRD if phase selective, you must be able to differentiate which peaks come from which phase. A single peak from phase A should be distinguished from a single peak from phase B of the same material. However, with all these considerations in mind regarding the selection of diffraction peak at high angles, it turns out that there is usually only one peak suitable to measure.

The Ag peaks were easily identified and measure with very low background noise present in the x-ray spectrum. The pattern was investigated at low angle, 20-90°, and also at higher angle, 90-160°. A peak was found around 156° and so a high intensity scan was conducted between 154° to 160°. Generally, higher ranged peaks are selected for XRD measurements because they

show the greatest amount of angular shift for a given crystal plane spacing change.

Preliminary XRD scan for W did show some presence of oxides since detection could be seen where there were small peaks in locations where $WO_3$ peaks should be. The W peaks were easily identified and measured with low background noise similar to that of Ag. The peak used to measure the strain on the coating was found between 131-132°. Consequently, a high intensity scan was taken between the ranges of 129-134°, just enough to have the entire peak scanned within this angle range. It is known that composition does affect the peak position in an XRD scan, but it is also known that not every peak shift is a sign of change in composition. Therefore, having various compositions of the W phase would not necessarily affect residual stress measurement. This is because we do not compare peak positions of strained versus the unstrained position, but rather, strained in different orientations of all the same composition. The different orientations are noted with the change in tilt angles of the sample or $\Psi$.

The four NiCr samples did not have well defined high angle peaks because of the resulting high background noise prevalent in NiCr coatings. The unusually large background noise is due to the high amount of Cr, 20% present, in the composition of the coating thus shifting the positions of the peaks as well as increasing the background noise level in the data. Another cause for this high background noise can be because of Cr or Ni scattering the x-rays once in the

material and making it more difficult for the detector to collect scattered x-rays thus increasing the noise level. The large peak width, also making it difficult to measure, is due to the plastic deformation of the coating. The measured peak was found between 151-152° and the high intensity scan was taken from 146 to 160°. The range of the NiCr scan was much larger than the W or Ag specimens because the peaks were not so well defined and it is also much wider than the other two coatings.

The NiCr and W crystal plane orientations were already given in the Bede ZDS database for $2\theta$ position so they did not have to be calculated. However, plane orientation for Ag were found in the database and had to be calculated using the formula [7]:

$$d_{hkl} = a/(\sqrt{h^2 + k^2 + l^2}) \tag{7}$$

where $d$ is calculated to be 0.787 when using Bragg's law, 1.54 as the radiation wavelength of CuKa1 source, and 78° as the diffraction angle. From the database, $a$ is equal to 4.086 and solving the equation for $h$, $k$, and $l$, it was found that there are two possibilities. These solutions are 333 and 511. It was concluded that there are two crystal plane orientations that give the same peak intensity at 156° for the Ag coating.

The $S_1$ and $1/2S_2$ were calculated using the Young's Modulus and Poisson's ratio from the bulk material for each corresponding specimen. Table 4 shows the calculated values for $S_1$ and $1/2S_2$ used in obtaining the residual stress.

| Sample | Young's Modulus (GPa) | Poisson's Ratio | $S_1$ | $1/2S_2$ |
|---|---|---|---|---|
| **NiCr** | 207 | 0.31 | -1.50E-06 | 6.33E-06 |
| **Ag** | 76 | 0.38 | -5.00E-06 | 1.82E-05 |
| **W** | 400 | 0.28 | -7.00E-07 | 3.20E-06 |
| **Mo** | 330 | 0.31 | -9.39E-07 | 3.97E-06 |

*Table 4. Young's Modulus, Poisson's Ratio, and calculated Crystallograhic Elastic Constants used to calculate strain for the XRD methodology technique*

Ni Filter used prior to the detector so it can decrease the intensity of Kalpha2 and increase the intensity of $K_{\alpha 1}$ in the measured diffraction peak. This particular filter material is able to decrease the intensity of $K_{\alpha 2}$ by a factor of 1/500, which is significant enough when determining peak intensity. There are filters made with different materials, but Ni is the best filter to use for a Cu tube such as the one used in this experiment. Each peak measured in the turbo basic program consists of two parts, $K_{\alpha 1}$ and $K_{\alpha 2}$, but $K_{\alpha 1}$ is typically more intense and larger. Even though the measure diffraction peak of a certain $\Psi$ has two peaks, $K_{\alpha 1}$ is regarded as the dominant peak and it is measured as one peak instead of two.

$$K_{\alpha} = (2K_{\alpha 1} + K_{\alpha 2}) / 3 \qquad (8)$$

There also exists $K_{\beta}$ in the diffraction measurement, but this not used in the peak measurement because the intensity of $K_{\beta}$ is much less than that of Kalph2 and Kal1 for that matter. Therefore, this $K_{\beta}$ is simply disregarded or ignored in the peak position calculation.

A monochromator can also be used as a way to decrease the intensity of the $K_{\beta}$ instead of using a filter system, but monochromators cause the

experimental set up to be more difficult and therefore is not often used. This type of apparatus can filter a particular wavelength or energy, monochromatic radiation with the use of a crystal. Turning the crystal allows selected wavelengths to be tuned or changed with great precision; such is the case for x-ray detection. Monochromators are usually made of $SiO_2$ or graphite.

The curve fitting program used to plot Kal1 data points and their intensity was done by a simple program called Turbobasic. This program has various types of curve fitting models, but the one used in the peak position calculations was the NTaylor series model. Once the peak has been measured, the results of the model can provide peak position, height, width and intensity. The most important calculation for determining stress in the sample is the peak position, specifically the change in peak position as you tilt the sample. Thus, position is the only value recorded and used in stress calculations since this provides information on the change in d-spacing in stressed material. The quantity of data points for each high angle diffraction peak for a given tilt angle can vary due to the amount of time given at each step and the range of the diffraction angle. For the Mo samples, 151 data points where measured to create the diffraction peak. For the NiCr samples, 141 data points were measured and for Ag and W it was slightly less than this.

## 2.3 Curvature Box Details

Thermal cycling of all the samples was done via curvature box and blow torched to a temperature of 200°C. This procedure was done to determine the change in curvature of the sample as a function of a change in temperature and then the stress of the film is calculated from the slope of the curvature versus temperature data. It is assumed that the modulus of the Mo will be the same for all Mo coatings even thought the substrate surface is difference and not all samples were vacuum heat treated. The calculation of the modulus will verify this assumption. The same procedure will be done with the NiCr coatings to assure that that the modulus is the same for all NiCr coatings. Figure 4 shows the Curveware program used in the curvature experiment. There were three lasers in the curvature box that helped determine the change in curvature of the substrate. Temperature of the substrate/coating was also monitored by several thermocouples in the curvature box.

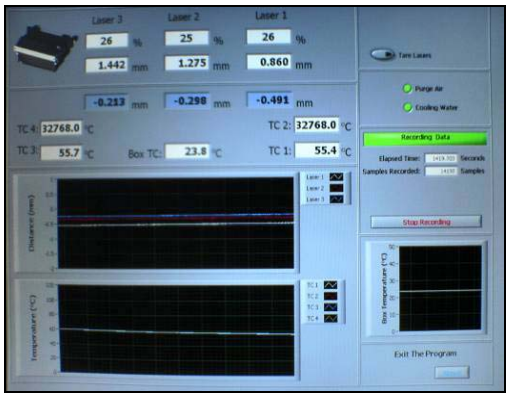


*Fig. 4. Curveware program for the curvature box experiment used to calculate residual stress along the entire coated sample*

Stoney Formula to get Film Stress:

$$\sigma_y = (1/6)(t_f/t_s^2)M_sR \quad (9)$$

where $M_s$ is the Biaxial modulus of the substrate, $R$ is the radius obtained from the curvature test, and $t_f$ and $t_s$ are the thicknesses of the film and substrate.

Biaxial modulus:

$$M_s = E_s/(1-v) \quad (10)$$

Biaxial modulus can be determined through the uniaxial modulus divided by one minus $v$ or the possion ratio of the material, in this case it would be steel.

Slope of Curvature Test (thermal cycling):

$$B = 6/E_s( t_s^2/t_f) E_f(\alpha_s - \alpha_f) \quad (11)$$

Through the manipulation of the Stoney Formula, it can be seen that the slope generated through the thermal cycling experiment can ultimately attain the modulus of the film. Modulus of the Film through manipulation of Stoney Formula:

$$E_f = (BE_s t_s^2)/[6t_f (\alpha_s - \alpha_f)] \quad (12)$$

## 2.4 Substrate Roughness and Residual Stress Correlation

This second experiment was created to investigate the relationship between substrate surface roughness and residual stress of thermally sprayed coating specifically Air Plasma Spray and High Velocity Oxy Fuel process. Increase in surface roughness was introduced in thermal spray industry to help improve adhesion between coating and substrate. There are three different

mechanisms associated with coating-substrate adhesion during thermal spray process: (1) mechanical interlocking effect, (2) physical bond, and (3) chemical-metallurgical bond [25]. The mechanical interlocking effect present in conventional thermal spraying processes indicates that adhesive strength increases with the improvement in the melting state of the spray particle and the increase in roughness of substrate surface [20-24]. Therefore, it is important to see how well the coating adheres to the substrate since it relates to curvature and ultimately residual stress. The residual stress is measure via XRD methodology as well as ICP technique and the results are compared. This experiment was done with both APS and HVOF with very thin coatings (30-50microns) to eliminate this argument between dominating stresses of peening or quenching. The results of this experiment should show the difference in peening and quenching effect by the comparison of HVOF versus APS and the residual stress present within there fairly thin coatings. This experiment should also help describe the effects of surface roughness on the residual stress of the coating.

Curvature (K) is proportional to coating adhesion through certain properties of the substrate and coating. The yield stress and stress relaxation mechanism of the coating are important. The surface roughness as well as the modulus of the substrate influences the curvature of the coating/substrate system.

Target coating thickness was 30-50microns or approximately 1 pass in both APS and HVOF process. The steel substrate coating thickness is

approximately 1.6mm. The steel substrate is cold rolled so there are already some residual stresses in the substrate therefore we eliminate this stress my placing some samples in a vacuum heat treatment (VHT). The VHT samples are placed in a vacuum of $10^{-6}$ torr and ramped up to 500°C for a one hour dwell and then ramped down to room temperature gradually.

| Sample | Psi (Tilt) | (+) 2θ | (+)δθ | (-) 2θ | (-)δθ |
|---|---|---|---|---|---|
| **NiCr (420) VHT 80psi HVOF** | 0 | 151.950 | 0.036 | 151.890 | 0.032 |
| | 26 | 151.810 | 0.035 | 151.870 | 0.038 |
| | 38 | 151.700 | 0.038 | 151.840 | 0.033 |
| | 49 | 151.750 | 0.051 | 151.710 | 0.039 |
| | 60 | 151.610 | 0.044 | 151.690 | 0.039 |
| **NiCr (420) VHT Polished HVOF** | 0 | 151.904 | 0.033 | 151.936 | 0.037 |
| | 26 | 151.860 | 0.044 | 151.954 | 0.036 |
| | 38 | 151.785 | 0.042 | 151.791 | 0.039 |
| | 49 | 151.713 | 0.043 | 151.877 | 0.037 |
| | 60 | 151.614 | 0.046 | 151.732 | 0.039 |
| **NiCr (420) VHT 40psi HVOF** | 0 | 151.928 | 0.038 | 152.040 | 0.034 |
| | 26 | 151.900 | 0.045 | 151.872 | 0.032 |
| | 38 | 151.827 | 0.043 | 151.890 | 0.035 |
| | 49 | 151.706 | 0.045 | 151.801 | 0.039 |
| | 60 | 151.633 | 0.051 | 151.718 | 0.043 |
| **NiCr (420) VHT As Recieved HVOF** | 0 | 151.986 | 0.036 | 152.014 | 0.042 |
| | 26 | 151.961 | 0.039 | 151.928 | 0.034 |
| | 38 | 151.862 | 0.041 | 151.882 | 0.035 |
| | 49 | 151.748 | 0.046 | 151.807 | 0.042 |
| | 60 | 151.678 | 0.045 | 151.688 | 0.045 |

*Table 5. NiCr Coating specimen shown with different tilt angles, 2θ positions with their deviations, spray process and crystal plane orientation*

Table 5 shows the different tilt angles and 2θ positions for the HVOF NiCr coatings with a crystal plane orientation of 420. The NiCr tilt angles used in

this second experiment are the same as that of the first because the coatings are the same. The 2θ positions are also relatively similar from the first experiment which would indicate that a similar peak position was selected. The time and steps at each tilt position are also the same as the first experiment, but are not seen in Table 5.

Table 6, seen below, has the same parameters shown in Table 5 except it is for the APS Mo samples used in the second experiment. There were four Mo coatings that were placed on vacuum heat treated (VHT) substrates and there were four Mo coatings that were placed on non-vacuum heat treated (NVHT) substrate. The vacuum heat treated substrates are assumed to be stress free while the non-vacuum heat treated substrates are assumed to have stress associated with the materials process of rolled steel as well as the grit-blasting procedure done prior to spraying. The 2θ position for the Mo coatings are noticeable different than that of the NiCr coatings because the suitable peak position for Mo is not that same as NiCr. Table 6 also indicates which Mo coatings were deposited on what type of substrate surface roughness, this information can be seen below the crystal plane orientation of the coating (320).

| Sample | Psi (Tilt) | (+) 2θ | (+)δθ | (-) 2θ | (-)δθ |
|---|---|---|---|---|---|
| **Mo (321) VHT 80psi APS** | 0 | 132.681 | 0.002 | 132.673 | 0.003 |
| | 26 | 132.630 | 0.002 | 132.685 | 0.002 |
| | 38 | 132.605 | 0.002 | 132.693 | 0.002 |

| | | | | | |
|---|---|---|---|---|---|
| | 49 | 132.586 | 0.002 | 132.733 | 0.002 |
| | 60 | 132.564 | 0.003 | 132.766 | 0.004 |
| **Mo (321) VHT Polished APS** | 0 | 132.688 | 0.002 | 132.692 | 0.003 |
| | 26 | 132.644 | 0.002 | 132.704 | 0.002 |
| | 38 | 132.626 | 0.002 | 132.706 | 0.002 |
| | 49 | 132.613 | 0.002 | 132.723 | 0.003 |
| | 60 | 132.601 | 0.003 | 132.752 | 0.004 |
| **Mo (321) VHT 40psi APS** | 0 | 132.711 | 0.003 | 132.704 | 0.003 |
| | 26 | 132.659 | 0.003 | 132.729 | 0.003 |
| | 38 | 132.647 | 0.002 | 132.725 | 0.002 |
| | 49 | 132.639 | 0.002 | 132.730 | 0.003 |
| | 60 | 132.629 | 0.003 | 132.765 | 0.005 |
| **Mo (321) VHT As Received APS** | 0 | 132.738 | 0.003 | 132.734 | 0.003 |
| | 26 | 132.684 | 0.003 | 132.754 | 0.002 |
| | 38 | 132.675 | 0.002 | 132.752 | 0.002 |
| | 49 | 132.659 | 0.003 | 132.757 | 0.002 |
| | 60 | 132.656 | 0.003 | 132.761 | 0.005 |
| **Mo (321) NVHT 80psi APS** | 0 | 132.708 | 0.003 | 132.710 | 0.003 |
| | 26 | 132.663 | 0.003 | 132.731 | 0.002 |
| | 38 | 132.648 | 0.002 | 132.730 | 0.002 |
| | 49 | 132.630 | 0.003 | 132.744 | 0.003 |
| | 60 | 132.629 | 0.004 | 132.783 | 0.004 |
| **Mo (321) NVHT Polished APS** | 0 | 132.676 | 0.003 | 132.681 | 0.003 |
| | 26 | 132.638 | 0.003 | 132.703 | 0.002 |
| | 38 | 132.613 | 0.002 | 132.707 | 0.002 |
| | 49 | 132.600 | 0.003 | 132.708 | 0.002 |
| | 60 | 132.602 | 0.003 | 132.754 | 0.004 |
| **Mo (321) NVHT 40psi APS** | 0 | 132.686 | 0.004 | 132.687 | 0.004 |
| | 26 | 132.641 | 0.004 | 132.712 | 0.004 |
| | 38 | 132.627 | 0.003 | 132.702 | 0.003 |
| | 49 | 132.606 | 0.003 | 132.724 | 0.004 |
| | 60 | 132.612 | 0.005 | 132.733 | 0.005 |
| **Mo (321) NVHT As Received APS** | 0 | 132.695 | 0.004 | 132.704 | 0.004 |
| | 26 | 132.644 | 0.005 | 132.710 | 0.004 |
| | 38 | 132.623 | 0.004 | 132.714 | 0.004 |
| | 49 | 132.617 | 0.004 | 132.724 | 0.004 |
| | 60 | 132.603 | 0.005 | 132.750 | 0.005 |

*Table 6. Mo Coating specimen shown with different tilt angles, 2θ positions with their deviations, spray process and crystal plane orientation*

A variety of substrate conditions were selected to help determine whether substrate surface roughness affected the final residual stress state, this can be seen in Table 7. Surface indicates the substrate roughness condition and $R_A$ is the

roughness averaged in microns for that particular surface. Vacuum heat treat, VHT, designates whether the substrate was stress free prior to coating or not.

| Process | Surface | $R_A$ [µm] | VHT | Coating | $T_{sub}$ [mm] | $T_{coat}$ [µm] |
|---|---|---|---|---|---|---|
| APS | As Received | 1 | Yes | Mo | 1.623 | 29.17 |
| APS | Polished | < 1 | Yes | Mo | 1.608 | 22.93 |
| APS | GB 40psi | 3 | Yes | Mo | 1.622 | 25.15 |
| APS | GB 80psi | 5 | Yes | Mo | 1.633 | 24.31 |
| APS | Polished | < 1 | No | Mo | 1.599 | 39.23 |
| APS | As Received | 1 | No | Mo | 1.624 | 34.62 |
| APS | GB 40psi | 3 | No | Mo | 1.628 | 32.04 |
| APS | GB 80psi | 5 | No | Mo | 1.609 | 34.01 |
| HVOF | Polished | < 1 | Yes | NiCr | 1.617 | 40.05 |
| HVOF | As Received | 1 | Yes | NiCr | 1.625 | 30.88 |
| HVOF | GB 40psi | 3 | Yes | NiCr | 1.624 | 34.80 |
| HVOF | GB 80psi | 5 | Yes | NiCr | 1.662 | 48.88 |

*Table 7. Various sample conditions used to determine the correlation between surface roughness and residual stress*

The substrate thickness, $T_{sub}$, was measured with a micrometer, but the coating thickness, $T_{coat,}$ was measured via Imagetool, a computer program. Imagetool was used since the coating thickness was so small that there was too much uncertainty in the micrometer reading. Imagetool was able to provide a more accurate coating thickness measurement than the micrometer.

It was necessary to etch the Mo coatings in order to determine the grain morphology and texture created by the APS process. We are looking for columnar solidification behavior within individual splats. Since the Mo coatings only have several splats we should be able to see corresponding grain growth. We will also try to determine crystallographic texture in the splats due to rapid solidification. The etchant composition used for the Mo coatings consisted of:

100ml water, 15g $K_3Fe(CN)_6$ and 5g NaOH. This particular composition is excellent for Mo and some of its alloys [10].

The etching of the NiCr samples is also possible, but smaller grain boundaries will be much more difficult to see than the larger grain boundaries present in the Mo samples. Etchant composition used in the NiCr coatings consisted of: 20ml $HNO_3$ and 80ml HCl. Coating is immersed in etchant for approximately 5-30 seconds then cleaned with deionized water. This etchant is made specifically for NiCr and alloys [11].

# Chapter 3: Results and Discussion

## 3.1 NiCr Process Map, W, and Ag

Once the XRD measurements were completed, figure 4 was constructed to investigate the $2\theta$ position versus the $\sin^2\Psi$ for the determination of independent stress tensor components. The graphs for W and Ag show a splitting of the positive and negative slopes due to the major difference between peak positions at these various orientations, unlike that of the four graphs of NiCr. The NiCr graphs show a similar trend with the positive and negative tilt angles, both having a downward slope of about the same slope value. The W and Ag coatings do not have comparable tilt angles, this peculiarity will be discussed further under the psi-splitting phenomenon.

The division between the positive and negative tilt angles indicates that these two specimens have anisotropic properties with the possibility of having a triaxial stress state while the NiCr coatings are anisotropic materials with biaxial stress state. Similarly, all the coatings are non textured material with small size crystallites and have moderate to low stress or composition gradient [7]. Crystallites are known as defect-free crystalline domains.

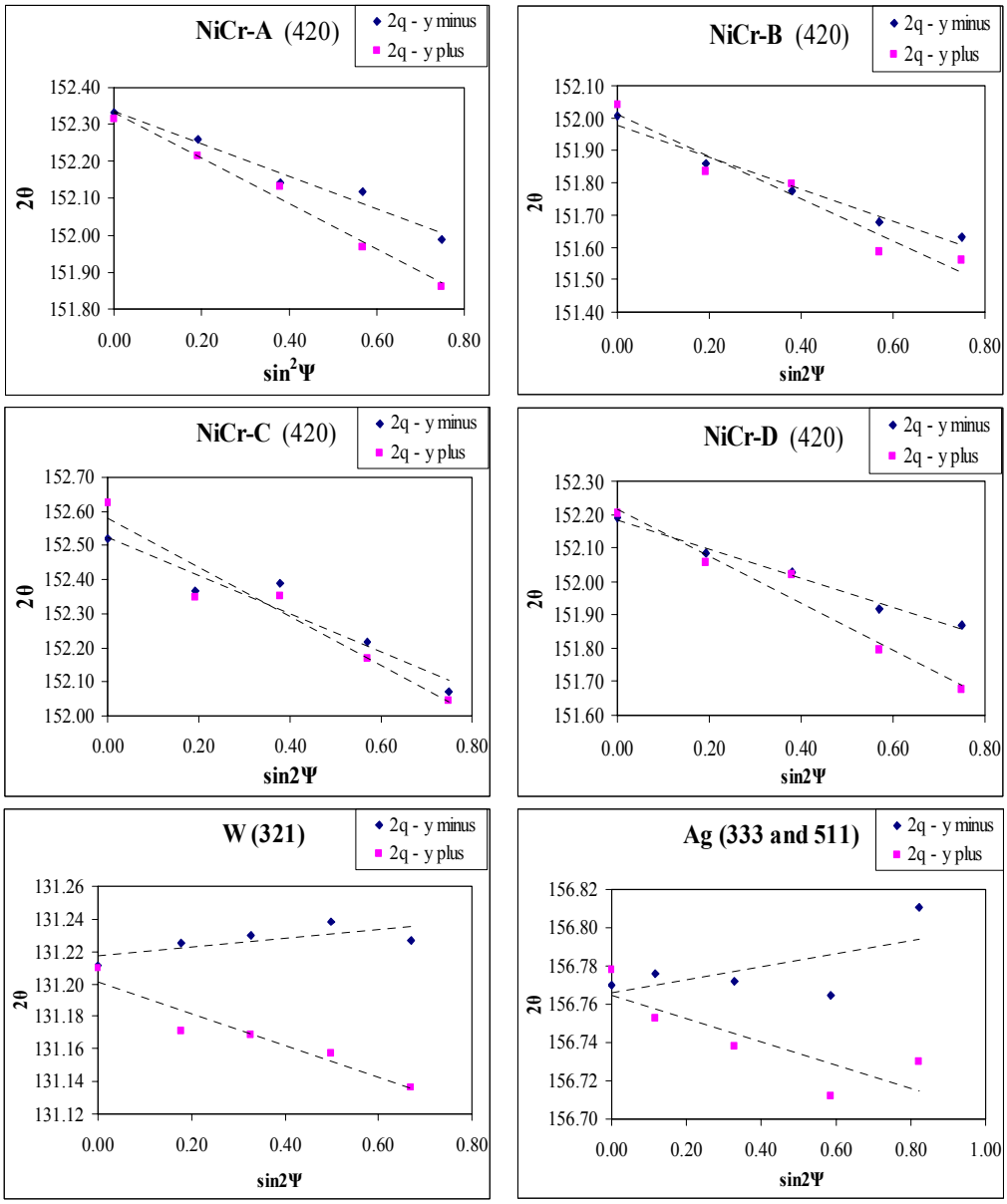


*Fig.5. Comparison of positive and negative peak position for the NiCr process maps and W and Ag coating specimens*

A comparison between the calculated residual stresses for the six specimens can be seen on Table 8, with the four HVOF NiCr samples having much greater stress than the APS sprayed W and Ag. The peening affect of the

HVOF process can attribute to this large difference in residual stress for the NiCr specimen versus the W and Ag. Since the W and Ag coating only obtain the quenching and thermal mismatch stress from the APS process, while the NiCr will get combination of quenching, thermal mismatch, and peening stress from the HVOF process. Given that XRD measurements are mainly on the first few layers of the coating (~50microns), the peening stress will dominate over the other two stresses, quenching and thermal, in the NiCr specimen also contributing to the higher residual stress.

| Specimen | Residual Stress (MPa) |
|---|---|
| **W** | 65.7 ±2.8 |
| **Ag** | 2.5 ±.2 |
| **NiCr-A** | 172.1 ±13.2 |
| **NiCr-B** | 199.9 ±10.9 |
| **NiCr-C** | 216.9 ±14.7 |
| **NiCr-D** | 191.3 ±12.3 |

*Table 8. Calculated residual stresses for W, Ag, and NiCr from XRD experiment*

The evaluation between the deposition, thermal, and residual stresses (from ICP and XRD measurement) for the four types of NiCr coatings sprayed with different parameters can been seen in table 6. A comparison graph of all four types of stresses found for the four types of NiCr parameters can also be seen in figure 2. All four NiCr samples have XRD residual stress that are tensile in nature compared to the ICP residual stress which have A and B in tension and C and D coatings in compression. It seems that residual stress from the XRD

measurement yields a higher value than that obtained from in-situ curvature process, which takes the average stress of the substrate/coating system.

| Sample | Young Modulus (GPa) | Deposition Stress (MPa) | Thermal Stress (MPa) | Residual stress-ICP (MPa) | Residual Stress-XRD (MPa) |
|---|---|---|---|---|---|
| **NiCr-A** | 190.1 | -69.84 | 106.79 | 36.95 | 178.3 |
| **NiCr-B** | 262 | -165.6 | 185.44 | 19.83 | 197.6 |
| **NiCr-C** | 190.4 | -145.41 | 106.9 | -38.51 | 214.9 |
| **NiCr-D** | 163.5 | -184.18 | 140.45 | -43.73 | 193.9 |

*Table 9. Moduli and residual stress data obtained from ICP sensor through insitu monitoring of curvature and temperature and XRD stress taken after spray*

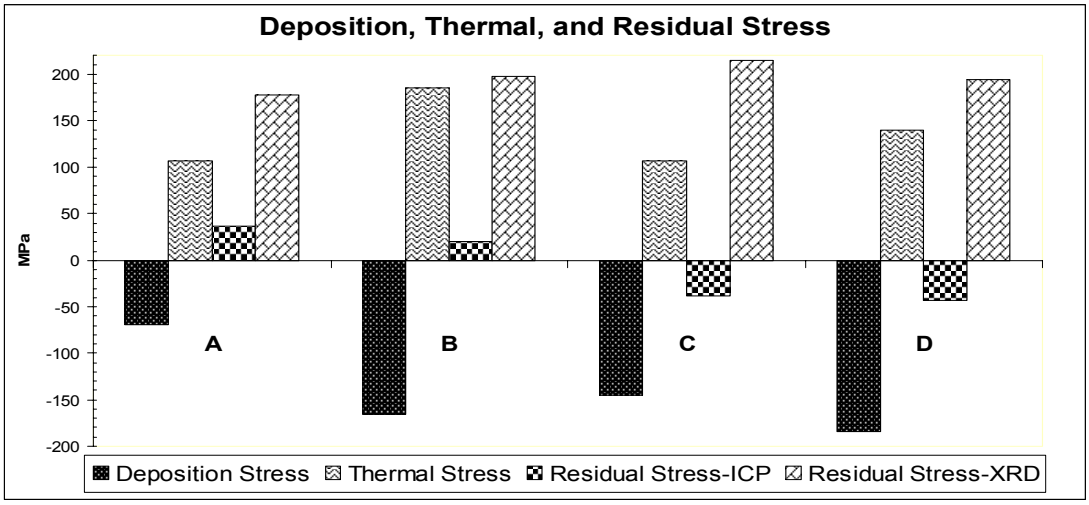


*Fig. 6. Ni20Cr: Deposition, Thermal and Residual stress values*

Likewise, XRD measurements are limited in there stress analysis since it can only take the surface layers into account and no deeper. Penetration depth of XRD is dependent on the source x-ray, in this study it was Cu as the source. Since coating thickness for the NiCr samples were approximately 300 microns, the residual stress taken from the XRD machine can only account for no more

than 50 microns from the surface. This still leaves in question an estimated 250 microns of coating stress to be determined. Fully understanding the relationships between peening, quenching and thermal stresses during the HVOF process must be known in order to completely describe the residual stress on these coatings. There is a possibility that peening would be more dominant in the deeper layers and so if you have a thick coating, this would be the principal stress measured. It can also be hypothesized that the quenching stress would be dominant on the top surface where no peening stress exists and therefore would be the principal stress at this layer. This large discrepancy between average residual stress from the ICP procedure and the surface residual stress of XRD can attribute to the major inconsistency between the two methods.

Future work on residual stress in thin film materials made by the thermal spray process should include coatings that are thin enough for X-rays to penetrate the entire coating to give you the through thickness residual stress. As long as the X-ray source is able to penetrate the entire coating material, then this thickness is arbitrary. Comparison of ICP and XRD methodology can only be done if you assume that both techniques are able to measure the same amount of coating stress.

## 3.2 Substrate Roughness and Residual Stress Correlation

The relationship between substrate roughness and residual stress of thick film coatings deposited via thermal spray is dependent on the stress release mechanisms that occur during the thermal spray process. These mechanisms affect the final stress in the coating and ultimately the coating/substrate system.

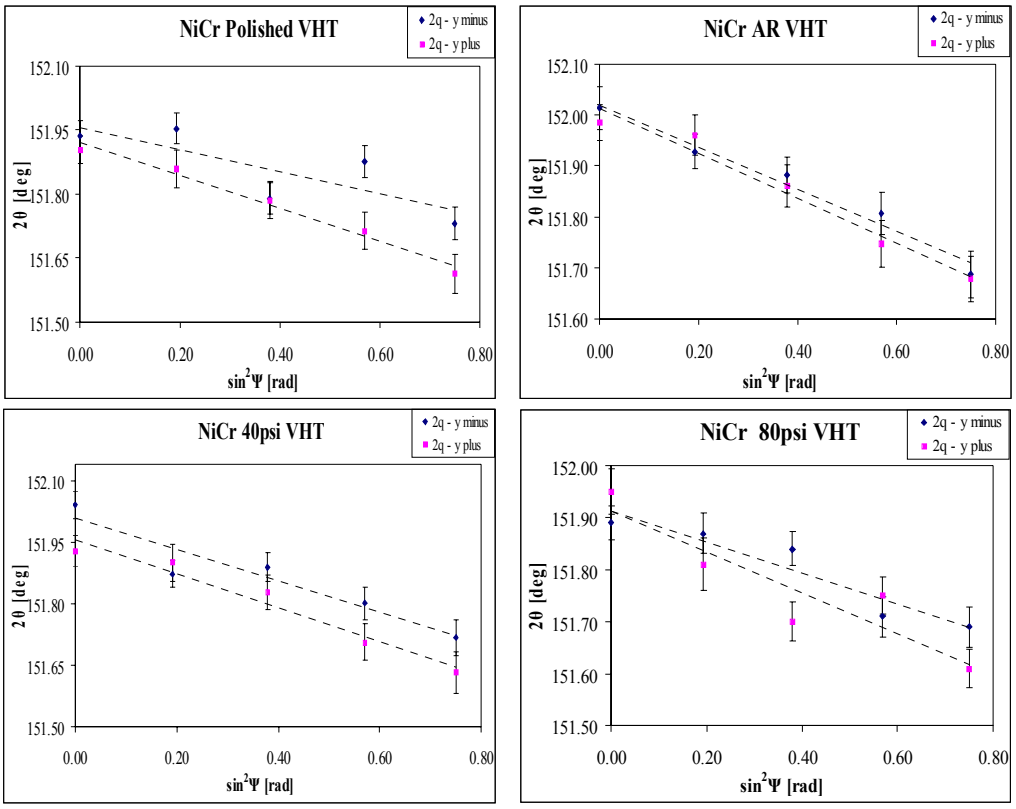


*Fig 7. Comparison of positive and negative peak position for NiCr coatings on four different vacuum heat treated substrate roughness*

Figure 6 shows the NiCr coatings on the four substrate roughness conditions from this experiment. These four NiCr graphs are very similar to that of the four NiCr graphs from the first experiment. The slopes on all four graphs

have the same general trend and slope value. The 40psi grit-blasted and as received substrate roughness have positive and negative tilt angle slopes almost parallel to one another. The polished and 80psi substrates are not as comparable.

The graphs for both VHT and NVHT Mo coatings are shown on Figure 7 and 16. There is a clear difference between the slopes of the Mo coatings versus that of the NiCr. The Mo coatings show what is called psi-splitting. This is when the positive and negative tilt angles have slopes that move in opposite directions. The significance of this phenomenon will be further discussed later in the paper.

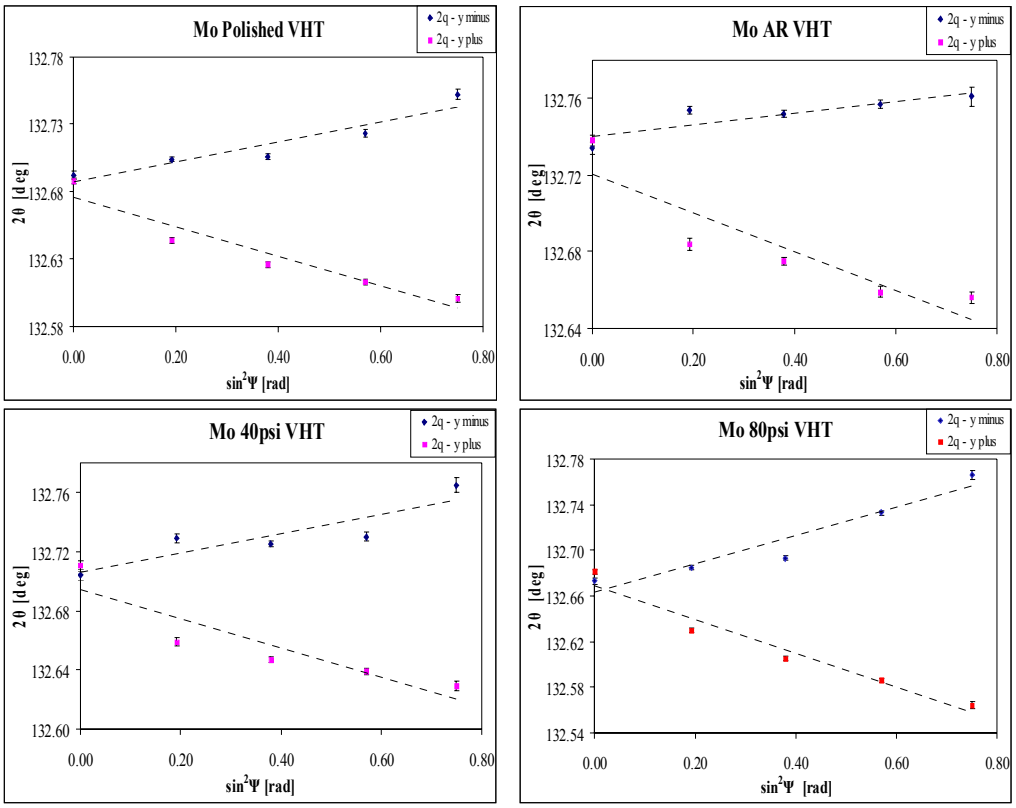


*Fig 8. Comparison of positive and negative peak position for Mo coatings on four different vacuum heat treated substrate roughness*

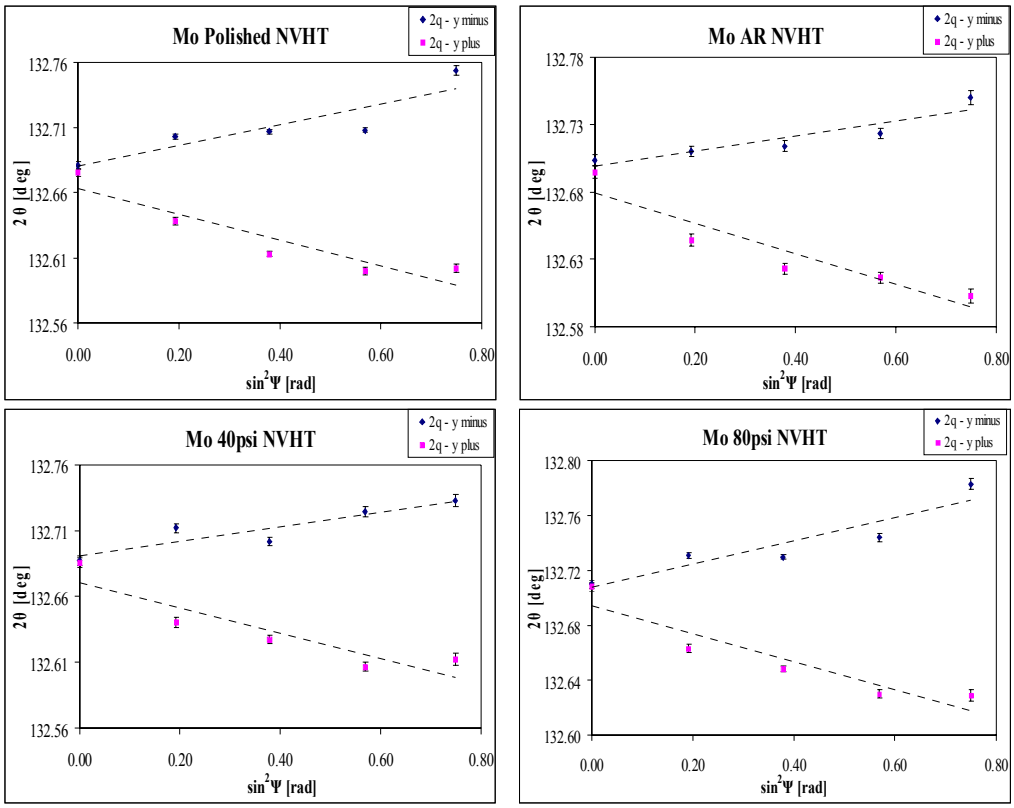


*Fig 9. Comparison of positive and negative peak position for Mo coatings on four different non-vacuum heat treated substrate roughness*

In the Mo samples the deviation in each peak positions is so small, in the order of thousandths, it can be ignored. This is evident by the small error bars barely visible on the graph and their values can be seen in Table 6. In the case of NiCr, the peak position deviation is on the order of hundredths and must be taken into consideration when doing the stress calculations. Stress calculations use a linear regression or best fit line model to determine the average peak position of the coating. Stress calculations with deviation in peak positions were calculated using the solver program in Microsoft excel. It takes into account the amount of

deviation in each peak position and computes the relative weight of the position and then averages it as a whole to give you the overall stress value with standard deviation. Table 10, below, show the XRD residual stress values for both NiCr and Mo coatings. The residual stress in the NiCr is much higher than that of the Mo which would indicate that the HVOF process induces stress different from that of the APS process. Comparing the stress values from the Mo coatings with substrates that were vacuum heat treated (VHT) and the ones that weren't show that there is no significance with having a stress free substrate prior to spraying.

| Process | Coating | Surface | VHT | XRD Stress [MPa] |
|---|---|---|---|---|
| APS | Mo | Polished | Yes | 17.1 ± 61.4 |
| APS | Mo | As Received | Yes | 33.9. ± 51.1 |
| APS | Mo | GB 40psi | Yes | 15.8 ± 56.5 |
| APS | Mo | GB 80psi | Yes | 11.5 ± 78.4 |
| APS | Mo | Polished | No | 9.3 ± 63.9 |
| APS | Mo | As Received | No | 27.1 ± 62.2 |
| APS | Mo | GB 40psi | No | 20.0 ± 57.1 |
| APS | Mo | GB 80psi | No | 8.5 ± 63.7 |
| HVOF | NiCr | Polished | Yes | 111.1 ± 26.7 |
| HVOF | NiCr | As Received | Yes | 146.5 ± 9.9 |
| HVOF | NiCr | GB 40psi | Yes | 137.5 ± 19.9 |
| HVOF | NiCr | GB 80psi | Yes | 119.4 ± 19.6 |

*Table 10. XRD residual stress values of HVOF NiCr and APS Mo with different substrate surface conditions*

The stress deviations in the NiCr coatings are much less than that of the actual residual stress values while this is not true for the Mo coatings. This is due to the fact that all the Mo coatings showed signs of psi-splitting. Since stress calculations are taken with the slope of both the positive and negative tilt angles, having one slope increase while the other decreases creates a large uncertainty.

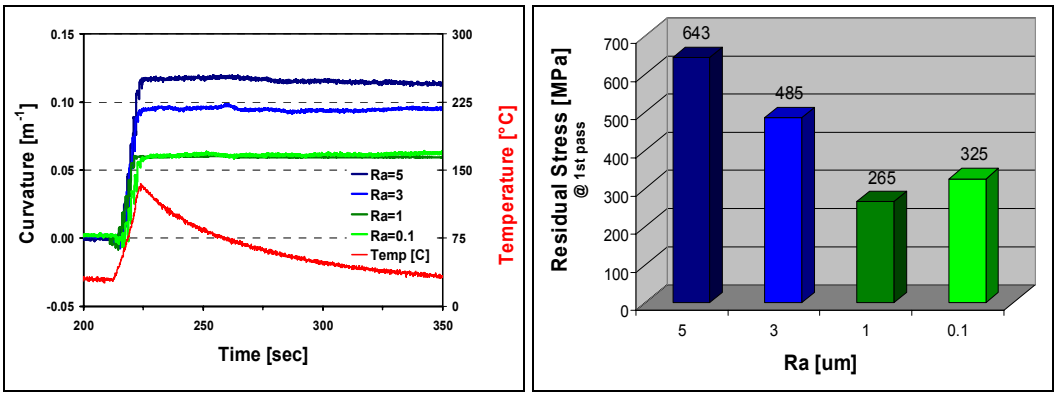


*Fig 10. ICP Residual Stress values for APS Mo on vacuum heat treated substrate*

Figure 9 shows the residual stress values for APS Mo on vacuum heat treated substrates using the ICP technique. The graph on the left shows curvature and temperature as a function on time and the graph on the right shows the residual stress values as a function of roughness average. It is evident that the substrate with the largest roughness has the largest stress and it decreases with decreasing roughness. The value for the 1micron $R_A$ is lower than that of the 0.1micron $R_A$ which seems odd, but if you look at the curvature data on the left, it shows that the 1micron and 0.1micron have almost identical curvature values. This could indicate that the difference in stress measurements is really within deviation values.

The results from the XRD technique show that all Mo coatings have similar stress values while the ICP technique shows that the substrate with a larger roughness average has the higher residual stress. The Mo coatings have stress values on the order of 10-20MPa with a deviation on the order of 50-70MPa because of the psi-splitting phenomenon.

The microstructure images seen in Figure 10, 11 and 12 were taken with a Zeiss microscope at 500x and 1000x magnification levels. Image analysis of these microstructures show several types of defects present. These defects are voids, minor oxidation, delamination and unmelted particles. Another point of interest is the coating/substrate material interface since we are studying the relationship between surface roughness and residual stress.

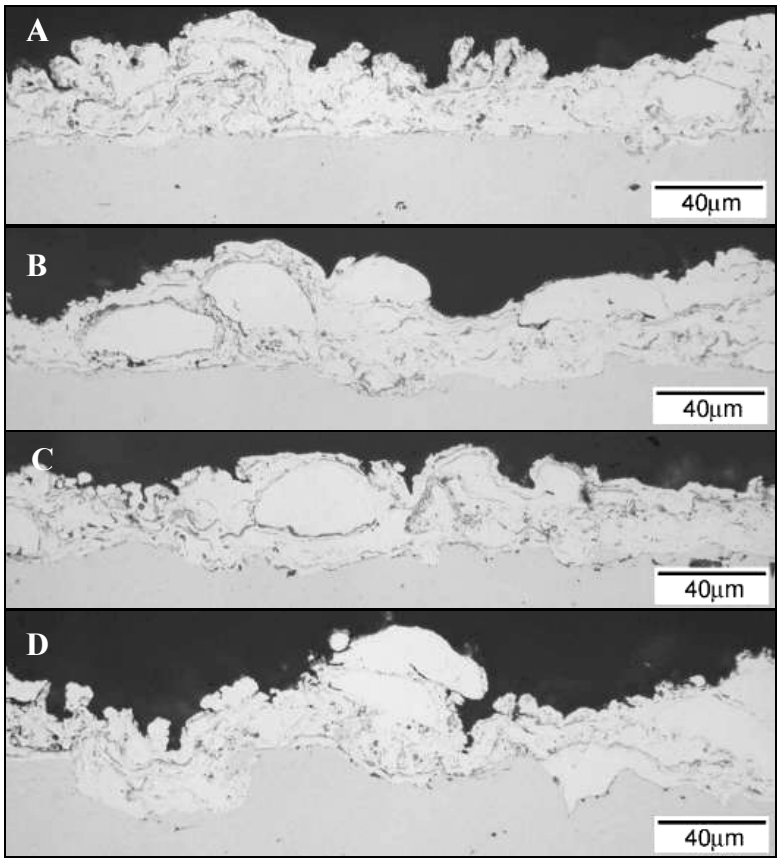


*Fig 11. Microstructure of NiCr coating on polished (A), as received (B), 40psi grit-blasted (C), and 80psi grit-blasted (D) substrate at 500x*

The NiCr coatings have a lot of unmelted particles, but the interface between coating and substrate look almost undistinguishable. This would indicate

good adhesion between coating and substrate. On the other hand, the Mo coatings on Figure 11 show not too many unmelted particles, but almost all have delaminated from the different substrate roughness conditions.

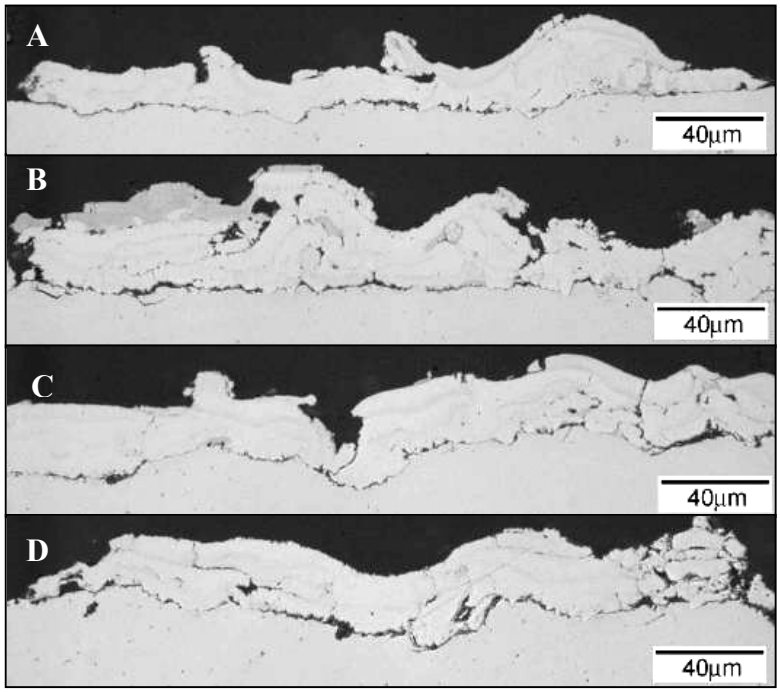


*Fig 12. Microstructure of Mo coating on polished (A), as received (B), 40psi grit-blasted (C), and 80psi grit-blasted (D) steel substrate at 500x*

The Mo coatings have lamellar microstructure but seem to have poor adhesion with the substrate, while the NiCr coatings do not have a lamellar structure with good coating adhesion to the substrate. The Mo coatings seem to have plenty of vertical cracks running along several splat thicknesses; this feature is not so evident in the NiCr. Image analysis shows that poor adhesion in the several types of substrate roughness was similar for all Mo coatings.

Figure 9 shows the polished and 80psi grit-blasted substrate with an etched Mo coating. The etchant was able to reveal columnular grain structure present in both coatings. The columnular grains are the fine vertical lines running up the several splat layers.

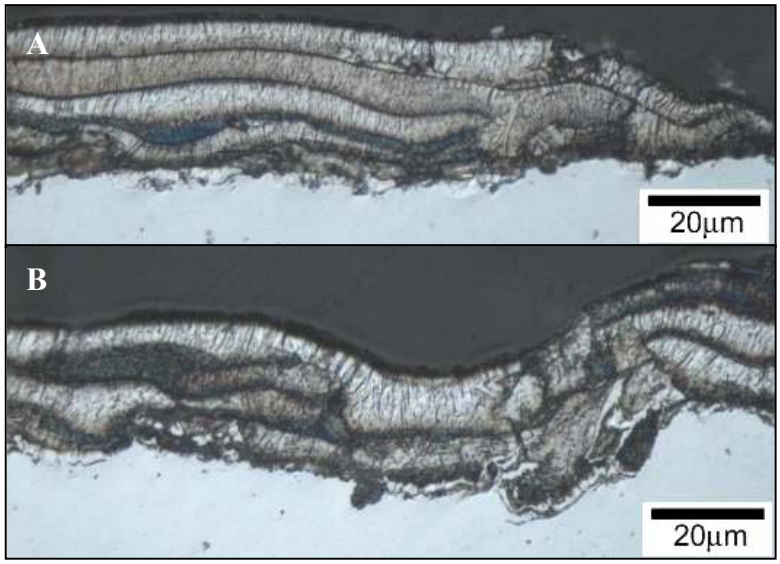


*Fig 13. Microstructure of etched Mo coating on polished (A) and 80psi grit-blasted (B) steel substrate at 1000x*

The columnular structure shows that the Mo coating has a preferred grain orientation created during the APS process. This structure is not typical for thermally sprayed coatings and is actually quite unusual.

Figure 10 and 11 show SEM images of the polished and 80psi grit-blasted Mo coatings. SEM was done to observe the discontinuity of the coating from a top view perspective as well as looking at the coatings with higher magnification. Both Figure 10 and 11 show the polished and 80psi grit-blast samples having poor continuity of coatings, seen by the darker shade of gray (substrate).

Comparison of Figure 10 and 11 shows that the coating structures for the polished and 80psi grit-blasted substrate are very similar; this is also valid by looking at Figure 8.

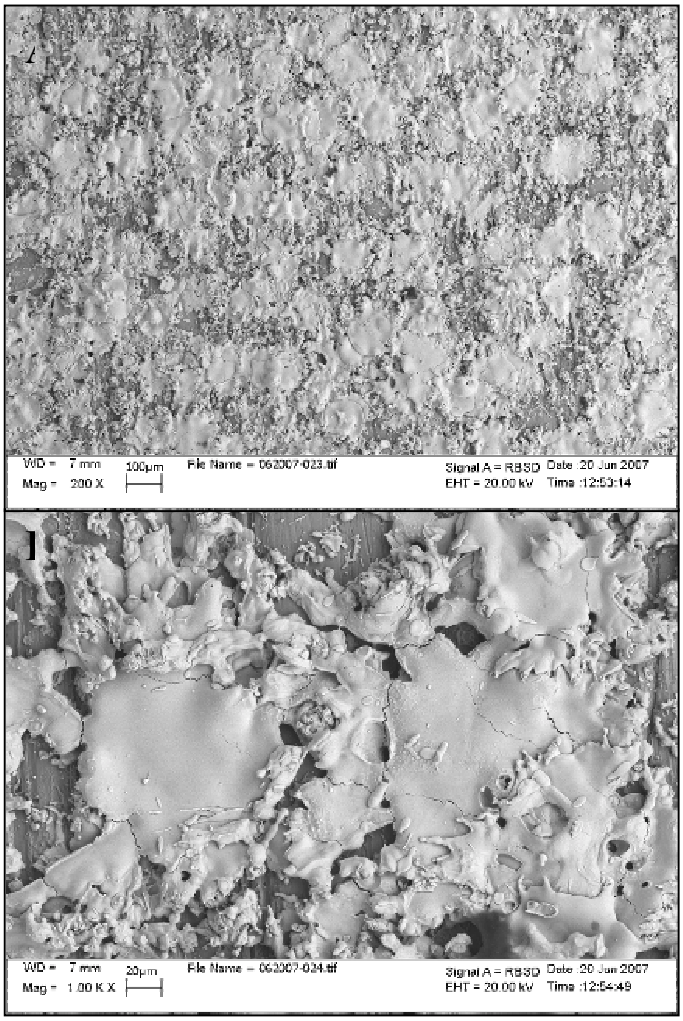


*Fig 14 SEM image of Mo coating on a polished steel substrate seen at low (A) and high (B) magnification*

There is plenty evidence of cracking in each splat as seen in Figure 10B and 11B even though coating on Figure 10 has done on a smooth substrate and Figure 11 was sprayed on a rough surface.

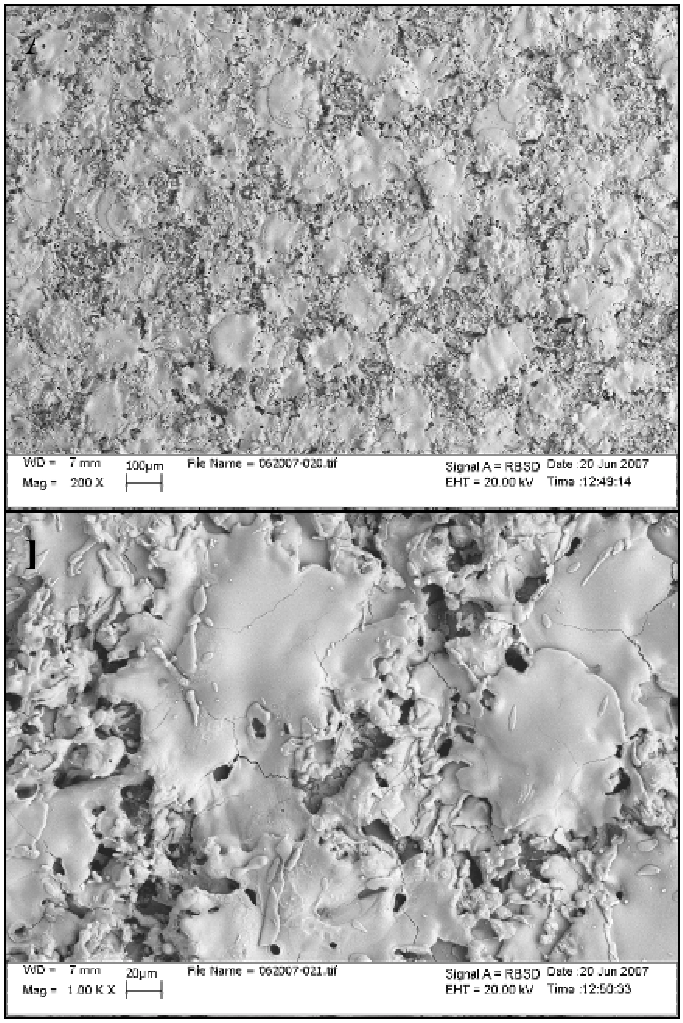


*Fig 15. SEM image of Mo coating on an 80psi grit-blasted steel substrate seen at low (A) and high (B) magnification*

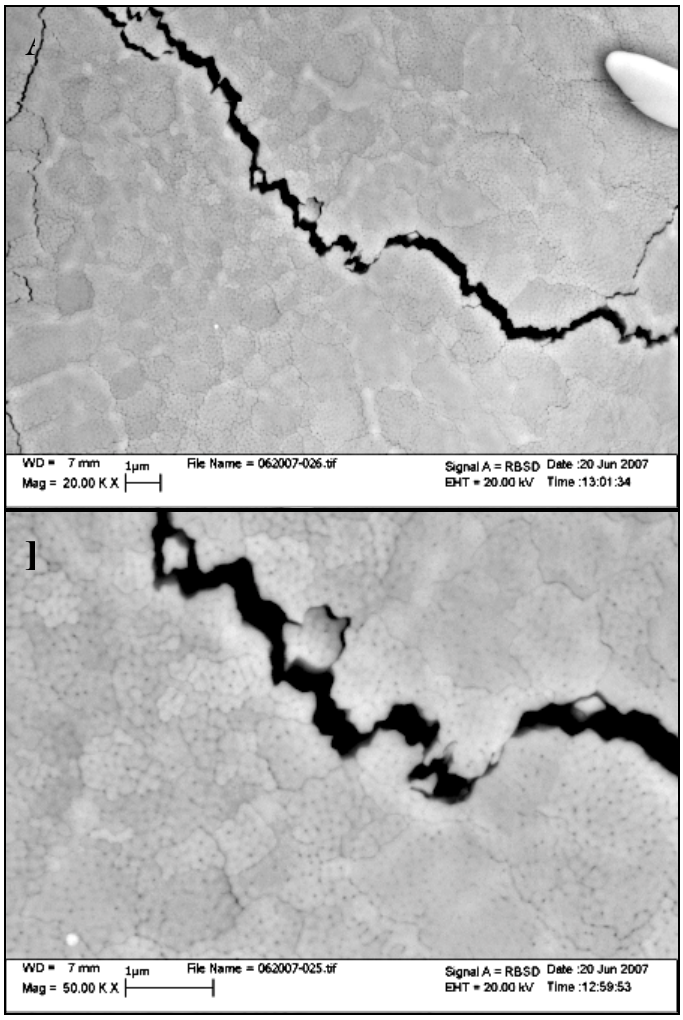


*Fig 16. SEM image of Mo coating with a crack propagating through the splat seen at low (A) and high (B) magnification*

Both cracking and delamination occurred in the Mo coating which means that the cohesion strength and adhesion strength of the material was less than that of the coating stress. The coating stress has to be less than the cohesion and adhesion strength of the material in order to prevent cracking or delamination. Cracking occurs when the cohesion strength fails and delamination occurs when adhesion strength of the coating fails.

There are many discontinuities between the splats for all Mo coatings, both horizontally and vertically, in all substrate roughness conditions. This could explain the low stress values observed by x-rays (10-20MPa), but the ICP data are quite significant (650-270MPa). ICP method shows that continuity or discontinuity of splats in the laterally direction can still have a significant affect on the final residual stress. The individual stress of each splat is what causes the curvature to change independent of lateral contact.

The XRD technique measures over tens of mm area of the sample and can only see the top splats not the ones below. The penetration depths of the Mo samples were less than 10microns and the penetration depth of the NiCr samples were around 12microns. The splat thickness is about 10microns which means XRD technique is only able to determine stress in the top splat and nothing below that. ICP method is able to take all the splat effects on the substrate and measure the change in curvature.

Further explanation for the psi-splitting occurrence has been studied and seen throughout the years, but no clear cut solution has been found. It has been stated that the reason for this line splitting is due to the principal stresses measured are not exactly perpendicular and in-plane to the surface of the material. The slight tilt in these three principal stress means that the out of plane stress, $\sigma_{zz}$, is non-zero [17-19]. For $\sigma_{zz}$ to be non-zero this would indicate that there is a stress value perpendicular to the free surface of the material and this can not be

the case. The out of plane stress must be zero in this material; therefore the in-plane stress should be non-zero, $\sigma_{xx,}\ \sigma_{zyy} \neq 0$. It is also assumed that the in-plane stress will be similar as you rotate the sample meaning you have a biaxial state of stress in the sample and not triaxial [1].

A possible solution for this line splitting problem was suggested by [12] and the author stated that rotating the sample with respect to the y-axis, instead of the x-axis. This is another thought to the problem, but you will simply have more measurements because of the larger number of tilt angles and so there is a larger number to average the entire surface. The technique used in this research is opposite of that suggested by [12] author. Discrete tilt angles are selected and a longer x-ray time at each angle is given to insure that there are enough data points gathered by the detector at this particular angle. This type of technique measures only a few grains over a longer period of time and so there is less averaging of peak diffraction. The other method suggests that you have more tilt angles measured a shorted time periods and so you will have more data to average the peak diffraction. It has been studied that the result for both these methods are comparable [12]. There are a few assumptions that have to be made when tilting the sample in say, the y-axis ($\varphi$), in stead of the customary x-axis ($\Psi$).

1. The stress throughout the sample volume is constant (No significant stress gradient).
2. The out of plane stress of the sample is zero.
3. The in-plane stresses are parallel to the surface.
4. The sample is elastic isotropic (Not the case for thermal spray coatings).

5. The material has a random distribution of crystal orientation (No preferred crystal grain direction).

In the case of assumption 1, if there exists some stress gradient in the coating [15, 16], then the best fit line representing the change in peak position as a function of $\sin^2\Psi$, or tilt angle, would in turn become a curved line. The curved line could either have a positive or negative slope, but it would not explain why the positive and negative tilt angles would have deviating curves instead of curves moving in the same direction.

Assumption 4 states that the sample must have elastic isotropic properties, but this is hardly the case for thermally sprayed materials. In fact, you have more of an elastic anisotropic material due to the overall columnular structure within each splat. This certain type of structure caused by the thermal spray process would suggest that there is a certain preferred crystal orientation in each splat because of the fact that when the splat rapidly cools, this creates the column or vertical orientation of the grains [14]. You have plastic deformation occurring during the deposition process and so you have different grain orientations that will be affected differently with the same stress applied to the entire sample. The assumption comes in to play when you presume that you have a homogeneous coating, but microscopically it is really inhomogeneous grain structure.

With regard to assumption 5, X-ray diffraction methodology works under the principal that you have plenty of crystal orientation that can be used to

measure the change the change in d-spacing for this particular direction. Since x-ray diffraction is a point measurement technique, you need to have a large number of possible crystal orientations in order to have enough measurements of this change in d-spacing. The XRD method can not be used for single crystals because of the above mentioned reasoning.

Another suggested solution to this line splitting problem is the fact that when you tilt the sample, then the focusing distance of both the source and detector with respect to the sample should either increase or decrease depending on the amount of tilt applied to the sample. With the x-ray diffraction technique used in this research, Bragg-Brentano method, the distance of the detector does not change when the sample is changed from its zero tilt position to either positive or negative tilt angle. Since the detector does not change its distance and only changes its radial position to ensure the best position to collect the x-rays, there is some scrutiny that this could be the cause of the line splitting. Furthermore, in the Bragg-Brentano method, the source tube in completely fixed, it neither moves radial or in distance with respect of the sample. So you have a defocusing of the x-rays when you apply a positive or negative tilt to the sample possibly causing this line splitting in peak position.

During the spray process, there is a slight angle in the deposition of the powder, but this can not be the cause of splitting because you always have the negative PSI increasing and +PSI decreasing. If this slight deposition angle was

the cause for splitting in the two peak positions, meaning the principal stresses are slightly tilted, then the results/evaluation should sometimes show that +PSI is decreasing and –PSI is increasing. You would see that the positive and negative tilt angles would show random increasing or decreasing of d-spacing (no preferred orientation). My results have shown that there is always a decreasing in d-spacing, peak position, with the +PSI of the sample and always an increase in the case where the sample has a negative tilt angle.

The slight angle in deposition proves that your material coating has plane strain property and not plane stress properties, meaning the out of plane stress in non-zero. One of the assumptions used in XRD methodology is that you don't have this plane strain condition but rather a plane stress condition. That being the case, it is therefore possible to that this triaxial stress state be the root of line splitting.

Furthermore, if you have this slight tilt in deposition, then the material coating can have a preferred crystal orientation [13] in this particular direction. XRD techniques also assume that you don't have this preferred orientation, but only a random crystal grain structure. Again, the flaw in the assumption where you possibly have a preferred crystal grain orientation could be a reason for line splitting. Table 11 shows the different in residual stress values when you are only measuring one the tilt angle slopes. It is clear that there is a difference in stress

values as well as states when you compare both the positive and negative tilt angles.

| Surface | VHT | XRD Stress (+Ψ) [MPa] | XRD Stress (-Ψ) [MPa] |
|---|---|---|---|
| Polished | Yes | 105.4 ± 11.3 | -71.1 ± 8.9 |
| As Received | Yes | 97.2 ± 16.1 | -29.3 ± 5.9 |
| GB 40psi | Yes | 94.7± 15.4 | -62.9 ± 11.8 |
| GB 80psi | Yes | 142.9 ± 10.8 | -119.9 ± 12.7 |
| Polished | No | 95.8 ± 13.8 | -77.2 ± 13.7 |
| As Received | No | 108.5 ± 14.7 | -54.2 ± 8.0 |
| GB 40psi | No | 93.0 ± 15.1 | -53.0 ± 8.7 |
| GB 80psi | No | 98.3 ± 13.4 | -81.3 ± 11.9 |

*Table 11. XRD residual stress values of positive and negative tilt angles for APS Mo with different substrate surface conditions*

Figure 16 compares the difference in slope of each of the four coatings produced. As you can see, the slope of each line is fairly similar to one another, but in Figure 17, the slope for the 80psi grit-blasted sample is slightly different.

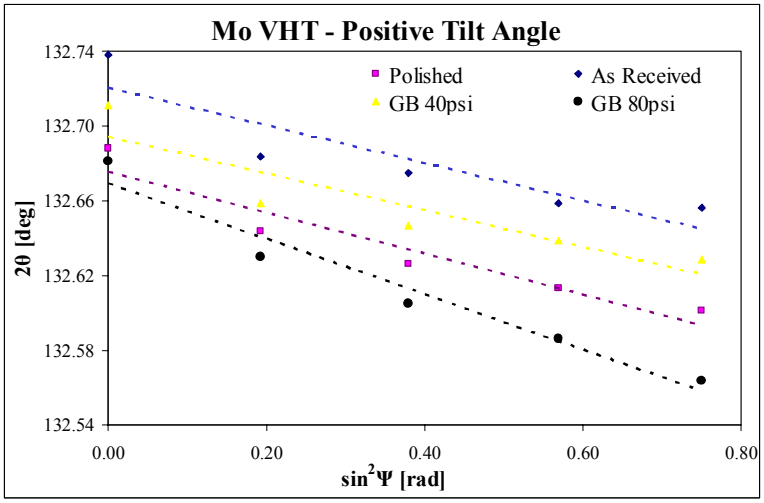


*Fig 17. Slopes of positive tilt angles for APS Mo coatings*

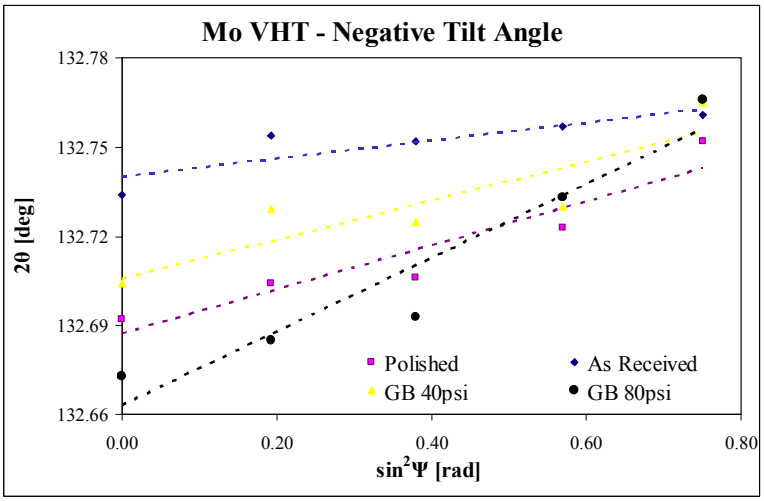


*Fig 18. Slopes of negative tilt angles for APS Mo coatings*

Looking at the residual stress values on Table 11 and comparing them to the Figures 17 and 18, you can see a correlation between the slopes and the stress values. The larger the slope angle is then larger the stress value.

# Chapter 4: Conclusions and Future Work

The residual stress measurement of an HVOF sprayed NiCr coating with four different parameters were obtained and discussed. Relationships between in-situ curvature measurement and x-ray diffraction measurements were analyzed and differences were scrutinized. Benefits and drawback for both stress measurement procedures were also argued. Residual stress for Ag and W coatings sprayed with APS were also examined and presented. A comparison between the residual stresses for the two types of spray procedures was also presented.

Coating adhesion and residual stress correlations were done with HVOF NiCr and APS Mo coatings having coating thicknesses less than 60microns. Assessment between coating adhesion and residual stress results between the HVOF and APS process were studied. The Mo coatings had two parameters, vacuum heat treat and non vacuum heat treat, that distinguished whether residual stress in the substrate prior to thermal spraying played any significance in the final residual stress of the coating/substrate system. Four different kinds of substrate roughness were investigated to determine how coating adhesion related to residual stress.

Possible future work on the adhesion/stress study would consist of spraying a thicker Mo coating but still with one pass to ensure continuity in the

coating. This would indicate increasing the powder feed rate but still keeping coating thickness relatively thin, approximately 30microns. Another possible experiment would be spraying scattered Mo splats on a substrate to determine whether roughness plays a role at the splat level. This test will depend on the curvature box and how well the sensors pick up deflections in the substrate. Further investigation on columnar grains of APS Mo would require an experiment with a five pass microstructure thickness and imaging comparisons between the lower layers of the coating to that of the upper layer. Similarities or contrasts between the $4^{th}$ and $5^{th}$ layer and the $1^{st}$ and $2^{nd}$ would help determine if the columnar grains were strictly created in coating thicknesses that are under 60microns or also above it.

# References


1. J. Matejick, S. Sampath, and J. Dubsky, X-ray Residual Stress Measurement in Metallic and Ceramic Plasma Sprayed Coatings, Journal of Thermal Spray Technology, Vol. 7 (No.4), Dec. 1998, p. 489-496
2. J. Matejick, S. Sampath, D. Gilmore, and R. Neiser, In-situ Measurement of Residual Stresses and Elastic Moduli in Thermal Sprayed Coatings. Part 2: Processing Effects on Properties of Mo Coatings, Acta Material, Vol. 51 (No.3), 2003, p. 873-885
3. J. Matejick, S. Sampath, In-situ Measurement of Residual Stresses and Elastic Moduli in Thermal Sprayed Coatings. Part 1: Apparatus and Analysis; Acta Material, Vol. 51 (No. 3), 2003, p. 863-872
4. T.W. Clyne and S.C. Gill, Residual stresses in Thermally Sprayed Coatings and Their Effect on Interfacial Adhesion – A Review of Recent Work, Journal of Thermal Spray Technology, Vol. 5 (No.4), 1996, p. 401-418
5. J. Matejick, Overview of Stress Determination Methods for Thermally Sprayed Coatings
6. A. Valarezo, Residual Stress measurement of HVOF Coatings by In-Situ Monitoring of Curvature
7. J. Lu, X-ray Diffraction Determination of Strains and Stresses, Handbook of Measurement of Residual Stresses, Society for Experimental Mechanics, Inc. 1996, p. 75-84
8. B. Cullity and S. Stock, Elements of X-ray Diffraction, Third Ed., Prentice Hall Inc. 2001
9. M. Hammond and D. Rowcliffe, Techniques for the Direct Observation of Structure and Imperfections, Techniques of Metals Research, Vol. II part 2, Interscience Publishers 1969, p. 719-749

10. G. Vander Voort, Meetallorgraphy Principles and Practice, Material Science and Engineering Serices, McGraw-Hill 1984, p. 661-663
11. ASM Handbook in Metallography and Microstructure, Vol. 9, 2004, p.1043-1044
12. I.C. Noyan and J.B. Cohen, Residual Stress- Measurement by Diffraction and Interpretation, Springer-Verlag, New York, 1987
13. S. Sampath and H. Herman, Rapid Solidification and Microstructure Development during Plasma Spray Deposition, J. Thermal Spray Tech., Vol. 5 (No.4), 1996, p445-456
14. H.P. Klug and L.E. Alexander, X-Ray Diffraction Procedures for Polycrystalline and Amorphous Materials, John Wiley & Sons, New York, 1974
15. I. Kraus and V.V. Trofimov, X-Ray Stress Measurement, Academia, Prague, 1988
16. I. Kraus and G. Gosmanova, X-ray diffraction Analysis of Macrostresses in Surface Layers of Metallic Materials, Met. Mater., Vol. 28 (No. 3), 1990, p75-79
17. H. Dolle and J.B. Cohen, Residual Stresses in Ground Steels, Metall. Trans. A, Vol. 11A (No. 1), 1980, p159-164
18. V.M. Hauk, R.W.M. Oudelhoven, and G.J.H. Vaessen, The State of Residual Stress in the Near Surface Region of Homogeneous and Heterogeneous materials after Grinding, Metall. Trans. A, Vol 13 (No. 7), 1982, p1239-1244
19. I.C. Noyan, Effect of Gradients in Multiaxial Stress States on Residual Stress Measurements with X-Rays, Metall. Trans. A, Vol 14 (No. 2), 1983, p249-258
20. M. Mellali, P. Fauchais, A. Grimaud, Surf. Coat. Technolo. 81, 1996, p275

21. P. Fauchais, M. Vardelle, A Vardelle, L. Bianchi, Ceram. Int. 22, 1996, p295
22. A.L. Hutson, M. Niinomi, T. Nicholas, D. Eylon, Int. J. Fatigue 24, 2002, P1223
23. C.C. Berndt, S.H. Leigh, Surf. Coat. Technol. 89, 1997, p213
24. S Amada, T. Hirose, Surf. Coat. Technol. 102, 1998, p132
25. Y.Y. Wang, C.J. Li, A. Ohmori, Influence of Substrate Roughness on the Bonding Mechanisms of High Velocity Oxy-Fuel Sprayed Coatings, Thin Solid films 485, 2005, p141-147